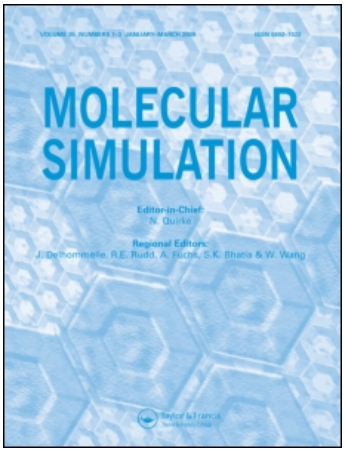

Molecular Simulation
Publication details, including instructions for authors and subscription information:
http://www.informaworld.com/smpp/title~content=t713644482

Modelling Gas Adsorption in Slit-Pores Using Monte Carlo Simulation

M. B. Sweatman[a]; N. Quirke[a]
[a] Department of Chemistry, Imperial College, London, UK

To cite this Article Sweatman, M. B. and Quirke, N.(2001) 'Modelling Gas Adsorption in Slit-Pores Using Monte Carlo Simulation', Molecular Simulation, 27: 5, 295 — 321
To link to this Article: DOI: 10.1080/08927020108031355
URL: http://dx.doi.org/10.1080/08927020108031355

Molecular Simulation, Vol. 27, pp. 295–321
Reprints available directly from the publisher
Photocopying permitted by license only

MODELLING GAS ADSORPTION IN SLIT-PORES USING MONTE CARLO SIMULATION

M.B. SWEATMAN and N. QUIRKE*

Department of Chemistry, Imperial College, South Kensington, London SW7 2AY, UK

(Received June 2001; In final form July 2001)

We discuss the use of Monte Carlo simulation to model the equilibrium adsorption of gases in slit pores. Databases of adsorption isotherms have been calculated for nitrogen, carbon-monoxide, methane and carbon-dioxide for a range of pressures, pore widths and temperatures. We discuss the implications of these results for materials characterisation procedures based on gas adsorption data.

Keywords: Monte Carlo simulation; Gibbs ensemble; Grand canonical ensemble; Graphitic slit pores; Adsorption isotherms; Materials characterisation

INTRODUCTION

In this paper we discuss the use of Monte Carlo simulation to model the equilibrium adsorption of gases in slit pores. While there are no perfect slit pore systems in Nature, the ideal slit pore model is a useful approximation to pores in real adsorbents of practical interest such as activated carbons.

Over the last twenty-five years the understanding of equilibrium fluid behaviour in restricted geometries has advanced considerably. Early theoretical models [1,2], such as the Langmuir and BET isotherms and the Kelvin equation, have been superceded by modern approaches such as density functional theory [3] (DFT) and Monte Carlo simulation [4–6].

*Corresponding author.

Indeed, one of the early applications of the Monte Carlo method to the study of physical adsorption on graphite by Rowley, Nicholson and Parsonage [7] in 1976 evaluated multi-layer methods, including the BET, Dubinin and FHH models, by comparing their predicted adsorption isotherms and heats of adsorption with simulation data for Lennard–Jones argon. None were considered to be satisfactory. In the present article we present an overview of current modelling procedures used to predict the adsorption of nitrogen (N_2), carbon-monoxide (CO), methane (CH_4) and carbon-dioxide (CO_2) in graphitic pores.

The Metropolis Monte Carlo technique [8] originated with Metropolis *et al.* in 1953 and was extended to the Grand-canonical ensemble by Norman and Filinov [9], Rowley *et al.* [10] and Adams [11]. Application to adsorption problems soon followed [7]. The Grand-canonical ensemble is the natural ensemble with which to study adsorption in open slit pores because the ensemble is specified by chemical potential, volume and temperature. In a slit pore adsorbate pressure is generally not equal to reservoir pressure and, unless experiments are performed with surface force apparatus [12], the natural comparison of simulation and experiment is made through the chemical potential. Gases adsorbed on surfaces have a non-uniform density profile in the direction normal to the surface. In order to properly describe the non-uniform fluid the fluid–fluid interaction must be accurate for fluid densities varying from gas to dense liquid. In developing our model potentials for gas adsorption we require that the potentials are capable of predicting bulk fluid phase coexistence properties. In this way we ensure that both vapour and liquid-like regions of adsorbed fluids are accurately described. The appropriate Monte Carlo technique for predicting bulk phase coexistence properties is the Gibbs ensemble method [13–15] invented by Panagiotopoulos in 1987 (and also applied to non-uniform fluids [16,17]).

This work describes molecular models for adsorption of N_2, CO, CH_4 and CO_2 in graphitic slit-pores. A great deal of work has been performed on these or similar systems [18–20] (as well as rare gases [21,22]). Our focus is on the determination of accurate two-body effective potentials calibrated against experimental data for bulk phase coexistence properties and adsorption on standard graphitic surfaces. We describe our modelling methodology in the next section together with an overview of the Gibbs and Grand-canonical ensemble simulation techniques. These techniques are used to fine-tune our effective molecular models. In the final section we describe our results for gas adsorption in graphitic slit pores for a range of pore widths and bulk pressures and comment on their implications for the characterisation of porous materials using gas adsorption isotherms.

METHODS

Molecular Models

We wish to determine useful molecular models for the adsorbates N_2, CO, CH_4 and CO_2. We model all repulsive–dispersive interactions with the Lennard–Jones (LJ) potential,

$$\varphi_{ij}^{LJ}(r_{ij}) = 4\varepsilon_{ij}((\sigma_{ij}/r_{ij})^{12} - (\sigma_{ij}/r_{ij})^{6}) \tag{1}$$

where σ_{ij} and ε_{ij} define the length and energy scale respectively of the interaction between LJ sites i and j, separated by r_{ij} on different molecules, and all electrostatic interactions with partial charges,

$$\varphi_{ij}^{C}(r_{ij}) = C_i C_j / 4\pi\varepsilon_0 r_{ij} \tag{2}$$

where i and j are charge sites (not necessarily coincident with any LJ sites), with charge C, on different molecules and ε_0 is the vacuum permittivity. We constrain cross-interactions between unlike LJ sites to be related to the pure interaction parameters by the Lorentz–Bethelot rules

$$\sigma_{ij} = (\sigma_{ii} + \sigma_{jj})/2; \qquad \varepsilon_{ij} = \sqrt{\varepsilon_{ii}\varepsilon_{jj}} \tag{3}$$

Adsorbate molecular models are constructed from at least one LJ site, with the position, $(\vec{r}_{0i})$, of each site fixed relative to the centre-of-mass and orientation of the molecule. The interaction between two (different) molecules, α and β, is then simply the sum of the individual LJ and charge pair-interactions,

$$\phi_{\alpha\beta} = \sum_{i\in\alpha j\in\beta} \phi_{ij}^{LJ} + \phi_{ij}^{C} \tag{4}$$

The total interaction energy between adsorbate molecules is then the sum

$$U_{gg} = U_{SR} + U_{LR}^{LJ} + U_{LR}^{C} = \sum_{\alpha<\beta} \phi_{\alpha\beta} \tag{5}$$

The interaction between a pair of molecules must be subject to a cut-off, r_c. When the distance between the centre-of-mass of two molecules is less than r_c, pair-interactions are calculated explicitly according to Eq. (4) and summed to give U_{SR}. However, for molecules outside this range LJ pair-interactions are treated in an average sense to give a long-range contribution, U_{LR}^{LJ}, to U_{gg}. Setting

the pair correlation function between molecules separated by more than r_c, to unity gives, for a bulk fluid,

$$U_{\mathrm{LR}}^{\mathrm{LJ}} = 2\pi \sum_{\alpha} \sum_{i_\alpha} \sum_{j} \rho_j \int_{r_c}^{\infty} \mathrm{d}r r^2 \phi_{ij}^{\mathrm{LJ}}(r) = \frac{8\pi}{3} \sum_{i} N_i \sum_{j} \rho_j \varepsilon_{ij} \left(\frac{\sigma_{ij}^{12}}{3r_c^9} - \frac{\sigma_{ij}^{6}}{r_c^3} \right) \quad (6)$$

where N_i is the number of sites of type i in the simulation and ρ_j is the density of LJ site type j in the corresponding bulk phase. The bulk or long-range density is required in advance and can be obtained from earlier simulations.

In this work we neglect the long-range contribution of electrostatic pair-interactions since it is always small relative to other contributions. For example, in liquid CO_2 at 265 K the contribution of electrostatic interactions is about 20% of the total interaction energy, and long-range LJ interactions contribute about 1% of the total interaction energy (using the cut-off defined in the Results section). However, for systems where long-range electrostatic interactions are thought to be significant (for example in water) methods such as the Ewald summation method [23–25] or the reaction field method [26] can be employed. When the distribution of partial charges of a molecule are quadrupolar, the long-range contribution can be determined in a similar fashion to the long-range LJ contribution (6), i.e. the long-range electrostatic interaction between two quadrupolar molecules can be approximated by the pair interaction of two quadrupolar moments and long-range pair correlation functions can be set to unity.

It is not uncommon to neglect long-range interactions altogether, leaving a small step discontinuity in the interaction between two molecules. To reduce the unwelcome effect of such discontinuities, the remaining short-range part of the potential can be shifted. Unless the range of each LJ and electrostatic pair-interaction is calculated individually to determine its short or long-range nature, rather than according to the separation of molecular centre-of-masses, very small discontinuities in the pair-interaction of two molecules will persist.

For the simple molecular gases that are the focus of this work we are free to choose interaction parameters σ_{ii}, ε_{ii}, C_i, $\vec{r}_{0i}$. We tune the interaction parameters for each adsorbate so that bulk liquid–gas coexistence properties fit experimental data, using Gibbs ensemble simulation to determine liquid–gas coexistence properties of a given model. We will show that with these molecular models we can reproduce bulk fluid experimental coexistence data for each adsorbate with reasonable accuracy. Clearly, for more demanding problems more accurate interaction potentials are required. For example, simulations of hydrocarbons often employ stretch and torsional potentials energy terms, while those of water sometimes employ hydrogen-bonding and polarisation terms.

We model the interaction between each molecular LJ site (i) and each graphite surface (s) by a Steele potential [27]

$$V_{i_\alpha s}(z_{i_\alpha}) = 2\pi\rho_c\Delta\varepsilon_{is}\sigma_{is}^2\left(\frac{2}{5}\left(\frac{\sigma_{is}}{z_{i_\alpha}}\right)^{10} - \left(\frac{\sigma_{is}}{z_{i_\alpha}}\right)^4 - \frac{\sigma_{is}^4}{3\Delta(z_{i_\alpha}+0.61\Delta)^3}\right) \quad (7)$$

where, for graphite, we set $\rho_c = 114\,\mathrm{nm}^{-3}$ and $\Delta = 0.335\,\mathrm{nm}$ and z_{i_α} is the distance of LJ-site i on molecule α from the plane of carbon atom centres in the first layer of the surface. The Steele potential is invariant in directions parallel to the surface and generally provides a good approximation to the potential obtained by summing individual LJ-surface atom pair interactions. The summed LJ potential can be very smooth in directions parallel to the slit, for example the Boltzmann factor for the methane-summed LJ interaction varies by at most 1% across the surface at the potential minimum at 298 K.

The ideal slit-pore potential is given by

$$V_{i_\alpha}^{\mathrm{ext}}(w, z_{i_\alpha}) = V_{i_\alpha s}(z_{i_\alpha}) + V_{i_\alpha s}(w - z_{i_\alpha}) \quad (8)$$

where w is the width between carbon atom centres in the first layer of opposing parallel surfaces. This gives

$$U = U_{\mathrm{gg}} + V_{\mathrm{g}} = U_{\mathrm{gg}} + \sum_\alpha\sum_{i_\alpha} V_{i_\alpha}^{\mathrm{ext}}(w, z_{i_\alpha}) \quad (9)$$

for the total interaction energy of a given microscopic state. This is the potential-energy function that we investigate with Monte Carlo simulation. For fluid in a slit-pore the long-range LJ contribution to U_{gg} is

$$\frac{1}{2}\left\langle \sum_\alpha\sum_{i_\alpha}\sum_j \int_{r_{ij}>r_c}^{\infty} \mathrm{d}\vec{r}_{ij}\rho_j(\vec{r}_j)g_{ij}^{(2)}(\vec{r}_i,\vec{r}_j)\phi_{ij}^{\mathrm{LJ}}(r_{ij})\right\rangle \quad (10)$$

where $\rho_j(\vec{r})$ is the singlet density [28] of site j, $g_{ij}^{(2)}(\vec{r}_i,\vec{r}_j)$ is the pair distribution function between sites i and j at $\vec{r}_i$ and $\vec{r}_j$, $r_{ij} = |\vec{r}_i - \vec{r}_j| = |\vec{r}_{ij}|$ and the angle brackets denote an ensemble average. By setting correlations between pairs of molecules to unity if they are separated by more than r_c we obtain from Eq. (10)

$$U_{\mathrm{LR}}^{\mathrm{LJ}} = \frac{1}{2}\left\langle \sum_\alpha\sum_{i_\alpha}\sum_j \int_{-\infty}^{\infty}\mathrm{d}z_j\rho_j(z_j)\int_{\max(|z_{ij}|,r_c)}^{\infty}\mathrm{d}r 2\pi r\phi_{ij}^{\mathrm{LJ}}(r)\right\rangle \quad (11)$$

The right-hand integral can be computed in advance for a range of values of the lower limit and $\rho_j(z)$ can be found from an earlier simulation. If $w<r_c$ or if $\rho_j(z)$ is not too inhomogeneous, then the molecular density further than

r_c from site i_α can be "smeared" to give a uniform density, ρ_j, within the slit. Then Eq. (11) becomes the sum of Eq. (6) and two further contributions, each calculated as

$$-4\pi\left\langle\sum_{\alpha}\sum_{i_\alpha}\sum_{j}\rho_j\varepsilon_{ij}\left(\frac{\sigma_{ij}^{12}}{90z_1^9}-\frac{\sigma_{ij}^{6}}{12z_1^3}+(r_c-z_2)\left(\frac{\sigma_{ij}^{12}}{10r_c^{10}}-\frac{\sigma_{ij}^{6}}{4r_c^4}\right)\right)\right\rangle;\quad \begin{matrix} z_1=\max(r_c,z), \\ z_2=\max(r_c,z), \end{matrix} \tag{12}$$

where $z = z_{i_\alpha}$ and $z = w - z_{i_\alpha}$ for the separate contributions. Calculation of this expression is much faster than Eq. (11). The same technique can be used to evaluate the long-range contribution to U_{gg} from quadrupolar pair interactions confined to a slit. Specialised techniques have been invented for treating confined fluids with more general electrostatic interactions [29].

The Steele-potential is a simplified model of reality. So, just as with fluid–fluid interaction parameters, the LJ site-surface interaction parameters, $(\sigma_{is}, \varepsilon_{is})$ must be tuned so that agreement between simulation, in this case in the Grand-canonical ensemble, and reference data is reasonable. In this work we choose gas-surface interaction parameters [30,31] calibrated from experimental adsorption isotherms of the gases on a low surface area porous carbon, Vulcan. Thus, our surface model is not intended to correspond to a perfect crystal of graphite, but instead to the irregular surface of porous carbons. Of course, such amorphous materials cannot be characterised by a single slit pore with fitted gas-surface interaction parameters, but previous work* has shown that characterising such materials in terms of poly-disperse arrays of slit-pores is reasonably successful. More demanding applications require more accurate surface models. For example, the vibrational modes of carbon nanotubes *in vacuo* have been simulated using a Tersoff–Brenner potential [32], which approximates the many-body and co-ordinated nature of carbon interactions in molecular carbon and hydrocarbon materials.

THE GIBBS ENSEMBLE

A Gibbs ensemble simulation simulates the coexistence of two bulk phases without simulating the interface between them. Each phase is simulated in a separate "box" with periodic boundary conditions and does not interact with the phase in the other box. Coexistence is guaranteed by the choice of Monte Carlo

*For example, see Ref. [30] and references therein.

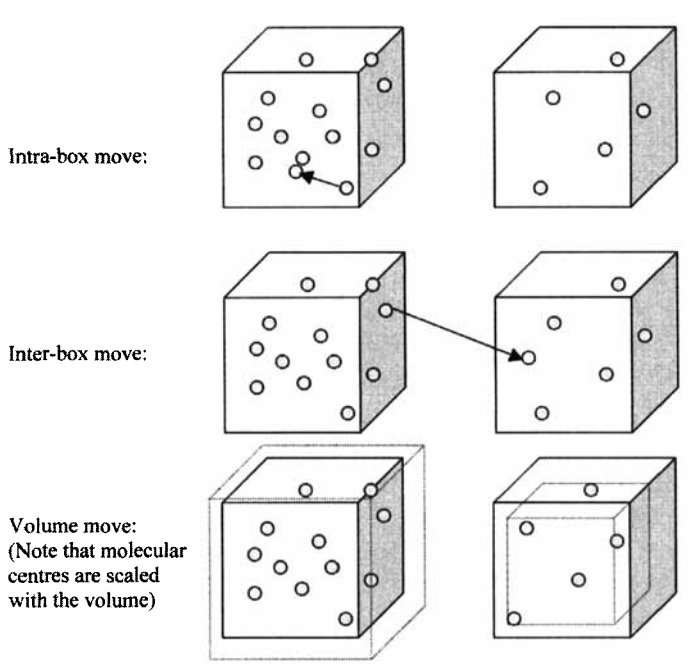

FIGURE 1 Schematic representation of Gibbs ensemble moves.

moves that produce the conditions for phase coexistence; equality of temperature, pressure and chemical potential. Intra-box moves (a molecule is moved randomly within the same box) equilibrate temperature, inter-box moves (a molecule is moved to a random location in the other box) equilibrate chemical potential and volume moves (volume is transferred from one box to the other) equilibrate pressure (see Fig. 1).

We performed Gibbs ensemble simulations for the pure fluids N_2, CO, CH_4 and CO_2 over a range of sub-critical temperatures. Our aim is to achieve good agreement between the results of Gibbs ensemble simulations and experimental data [33–40], namely the liquid and gas densities and pressure at coexistence, by adjustment of the effective interaction parameters $(\sigma_{ii}, \varepsilon_{ii}, C_i, \vec{r}_{oi})$ for each adsorbate. We employ long-range corrections for LJ interactions only.

For each simulation we started the two simulation boxes with lattice-like configurations, the density of one box being 50% greater than the other box. The dimensions of each box are chosen so that their volumes are approximately equal at equilibrium and to ensure that the box length is never less than the cut-off radius. We choose different moves at random with pre-defined probability. For a simulation with N molecules the relative probabilities for intra-box, inter-box and volume moves are 1, a and $1/N$ respectively. The value of a is fixed so that the

number of accepted inter-box moves is generally not less than 10% of the number of accepted intra-box moves. Thus, a is typically in the range 1–100, with higher values for denser liquid phases. Intra-box and inter-box moves are performed by choosing a molecule at random from both boxes. An intra-box move is performed by displacing a molecule in a random direction by a distance chosen randomly from a pre-defined interval. The molecule is then rigidly rotated about a randomly chosen Cartesian axis by an angle chosen randomly from a pre-defined interval. An inter-box move is performed by destroying a molecule in one box and then creating it at a random position with random orientation in the other box. A volume move is performed by taking a step on $\ln(V_{b1}/V_{b2})$ with step-length chosen at random from a pre-defined interval (the subscripts b1 and b2 refer to box 1 and box 2 respectively). When a box changes volume, the location of the centre of each molecule is scaled accordingly so that volume loss corresponds to compression and volume gain corresponds to decompression. The maximum step-size of intra-box and volume moves is fixed so that about 50% of these moves are accepted. We find that these move selection rules generally result in quick and stable phase separation.

Intra-box moves are accepted with probability

$$\min\{1, \exp[-\beta\Delta U]\} \tag{13}$$

where $\Delta U = U^n - U^m$ is the difference in total energy between the trial (n) state and the current (m) state. The total energy of a given state is the sum of the energies of the individual boxes. Inter-box moves are accepted with probability

$$\min\left\{1, \frac{N_{b1}V_{b2}}{(N_{b2}+1)V_{b1}}\exp[-\beta\Delta U]\right\} \tag{14}$$

if the molecule is to be moved from box 1 to box 2. The volume move acceptance rule must take account of the logarithmic volume-step selection rule and is

$$\min\left\{1, \left(\frac{V_{b1}^n}{V_{b1}^m}\right)^{N_{b1}+1}\left(\frac{V_{b2}^n}{V_{b2}^m}\right)^{N_{b2}+1}\exp[-\beta\Delta U]\right\} \tag{15}$$

These selection and acceptance rules satisfy microscopic reversibility and guarantee that the limiting distribution of states conforms to the Boltzmann distribution [4,5].

THE GRAND-CANONICAL ENSEMBLE

A Grand-canonical ensemble simulation simulates a single phase at a given set of chemical potentials (one for each distinct species of molecule) $\{\mu_\alpha\}$, volume and temperature. Equilibrium is achieved by careful choice of intra-box moves (temperature equilibrium), and creation and annihilation moves (chemical potential equilibrium). Our aim is to generate databases of the adsorption of gases in a range of pore widths over a wide range of pressures. These databases can then be used, together with the poly-disperse slit-pore model, for the characterisation of porous carbons. We use Grand-canonical ensemble simulation to construct the databases.

Grand-canonical ensemble simulations are initialised with either an empty box or a configuration of molecules obtained from an earlier simulation. For simulations in a slit pore the width of the box is fixed. The remaining free dimensions of the box are chosen to ensure sufficient molecules within it at equilibrium and are never less than twice the cut-off range. We perform three different types of move at random with equal probability. An intra-box move is performed in an identical manner to an intra-box move in a Gibbs ensemble simulation. A creation move is performed by creating a molecule at a random position with random orientation in the box. An annihilation move is performed by choosing a molecule in the box at random and deleting it from the simulation. The maximum step-size of intra-box moves is fixed so that about 50% of these moves are accepted.

Intra-box moves are accepted according to Eq. (13). Creation and annihilation moves are accepted with probability

$$\min\left\{1, \frac{V\Lambda_\alpha^{-3}}{N+1}\exp[\beta(\mu_\alpha - \Delta U)]\right\} \tag{16}$$

and

$$\min\left\{1, \frac{N+1}{V\Lambda_\alpha^{-3}}\exp[\beta(-\mu_\alpha - \Delta U)]\right\} \tag{17}$$

respectively. These selection and acceptance rules satisfy microscopic reversibility and guarantee that the limiting distribution of states conforms to the Boltzmann distribution [4,5]

SOME THERMODYNAMICS

The grand potential, Ω, is defined statistically in terms of the grand partition function, Ξ, as

$$\Omega = -k_B T \ln \Xi \tag{18}$$

which, with the Boltzmann distribution, gives

$$\Omega = \langle F \rangle - \sum_\alpha \mu_\alpha \langle N_\alpha \rangle = \langle E \rangle - T\langle S \rangle - \sum_\alpha \mu_\alpha \langle N_\alpha \rangle \tag{19}$$

where F, E and S are the Helmholtz free energy, internal energy and entropy respectively and Ω is minimized at equilibrium [41]. In the thermodynamic limit, we can drop the ensemble average notation, $\langle\,\rangle$, and Ω acquires non-analyticities along the loci of phase transitions [41]. In this work we focus on the behaviour of fluid adsorbed in solid slit pores. The model potential (7) approximates the solid surface as an effective external potential. So, we construct Gibbs dividing surfaces [42,43] at $z = 0$ and $z = w$ and effectively ignore the contribution of the surface or reservoir to Eq. (19). For a planar adsorbed system with area A and width w, an infinitesimal change in energy is written [43]

$$\mathrm{d}E = T\,\mathrm{d}S + \sum_\alpha \mu_\alpha \,\mathrm{d}N_\alpha - \int_0^w P_T(z)\,\mathrm{d}z\mathrm{d}A - AP_N\,\mathrm{d}w \tag{20}$$

where P_T and P_N are the transverse (parallel) and normal components of the pressure tensor respectively. The transverse component varies with z but the normal component does not. For fluid adsorbed on an isolated surface $P_N = P$ while for a bulk system all components are equal to P. With Eq. (19) this gives

$$\mathrm{d}\Omega = -S\,\mathrm{d}T - \sum_\alpha N_\alpha \,\mathrm{d}\mu_\alpha - \int_0^w P_T(z)\,\mathrm{d}z\mathrm{d}A - AP_N\,\mathrm{d}w \tag{21}$$

For fluid at given T and w we obtain two useful routes to the grand potential. The first by integrating along a continuous isotherm

$$\mathrm{d}\Omega = -\sum_\alpha N_\alpha \,\mathrm{d}\mu_\alpha \tag{22}$$

and the second from P_T

$$\Omega = -A\int_0^w P_T(z)\,\mathrm{d}z = -A(wP + \gamma) \tag{23}$$

For a bulk system one has from Eq. (21)

$$dP = \sum_{\alpha} \rho_{\alpha} \, d\mu_{\alpha}; \quad \gamma = 0 \tag{24}$$

Equation (21) requires the non-analyticities that develop in Ω in the thermodynamic limit to be manifest in the behaviour of S, N_{α}, P_{T} and P_{N}. At first-order phase transitions [44], S, N_{α} and P_{N} display step-discontinuities, while the average transverse pressure displays a step-discontinuity in its gradient with respect to T, μ_{α} and w. So, just as the bulk density is the order-parameter that signals the bulk liquid–gas phase transition, the average pore density, $\rho_{\alpha} = N_{\alpha}/Aw$, is the order parameter for phase transitions in a slit-pore. Similarly, just as bulk pressure is maximised at equilibrium, the average transverse pressure is also maximised at equilibrium.

Because we reduce all gas–gas interactions to effective pair-potentials the components of the pressure tensor can be defined microscopically from the pair-virial [4,5]. The v-component for a planar geometry is (according to the "Irving and Kirkwood" definition [42])

$$p_v(z) = k_{\mathrm{B}} T \sum_{\alpha} \rho_{\alpha}(z) - \frac{1}{2A} \left\langle \sum_{\alpha \neq \beta} \sum_{i_{\alpha} j_{\beta}} \left(\frac{d\phi_{ij}^{\mathrm{LJ}}}{dr_{ij}} + \frac{d\phi_{ij}^{C}}{dr_{ij}} \right) \frac{v_{\alpha\beta} v_{ij}}{r_{ij} |z_{ij}|} \theta\left(\frac{z - z_i}{z_{ij}} \right) \theta\left(\frac{z_j - z}{z_{ij}} \right) \right\rangle \tag{25}$$

where $\rho_{\alpha}(z)$ is the singlet density of molecular species α, $v_{\alpha\beta}$ and v_{ij} are the v–components of the vectors between the centres of molecules α and β and the sites i and j respectively and θ is the Heaviside step-function. Using Eq. (23) gives

$$\Omega = k_{\mathrm{B}} T \sum_{\alpha} \left\langle \langle N_{\alpha} \rangle - \langle \sum_{\alpha \neq \beta} \sum_{i_{\alpha} j_{\beta}} \left(\frac{d\phi_{ij}^{\mathrm{LJ}}}{dr_{ij}} + \frac{d\phi_{ij}^{C}}{dr_{ij}} \right) \frac{x_{\alpha\beta} x_{ij} + y_{\alpha\beta} y_{ij}}{4 r_{ij}} \right\rangle \tag{26}$$

Of course, these expressions are useful for the short-range part of any pair-potential only. Long-range LJ corrections to Ω, obtained with the same approximations used in Eq. (12), are two contributions calculated as

$$2\pi \left\langle \sum_{i_{\alpha}} \sum_{j} \rho_j \varepsilon_{ij} \left(\frac{m^3}{3} \left(\frac{\sigma_{ij}^{12}}{r_{\mathrm{c}}^{12}} - \frac{\sigma_{ij}^{6}}{r_{\mathrm{c}}^{6}} \right) - 6m \left(\frac{\sigma_{ij}^{12}}{5 r_{\mathrm{c}}^{10}} - \frac{\sigma_{ij}^{6}}{4 r_{\mathrm{c}}^{4}} \right) - \frac{1}{45} \left(\frac{\sigma_{ij}^{12}}{m^9} - \frac{\sigma_{ij}^{12}}{z^9} \right) + \frac{1}{6} \left(\frac{\sigma_{ij}^{6}}{m^3} - \frac{\sigma_{ij}^{6}}{z^3} \right) \right) \right\rangle \tag{27}$$

with $m = \min(z, r_{\mathrm{c}})$ and $z = z_{i_{\alpha}}$ and $z = w - z_{i_{\alpha}}$ for the two contributions. This expression can be calculated either for each configuration (and then averaged) or at the end of the simulation using the singlet density, $\rho_i(z)$. A similar expression can be obtained for the long-range contribution from quadrupole pair interactions. The

contribution of more general electrostatic interactions to the components of the pressure tensor and the grand-potential can be found using the Ewald summation method [45] or other methods [29]. For a uniform fluid, all components of the pressure tensor are equal and the short-range contribution to P is

$$P_{\mathrm{SR}} = k_{\mathrm{B}}T\sum_{i}\langle\rho_i\rangle - \frac{1}{2V}\left\langle\sum_{\alpha\neq\beta}\sum_{i\alpha j\beta}\left(\frac{\mathrm{d}\phi_{ij}^{\mathrm{LJ}}}{\mathrm{d}r_{ij}} + \frac{\mathrm{d}\phi_{ij}^{C}}{\mathrm{d}r_{ij}}\right)\frac{x_{\alpha\beta}x_{ij} + y_{\alpha\beta}y_{ij} + z_{\alpha\beta}z_{ij}}{3r_{ij}}\right\rangle \quad (28)$$

The long-range contribution of LJ pair interactions is then

$$P_{\mathrm{LR}}^{\mathrm{LJ}} = 8\pi\sum_{ij}\rho_i\rho_j\varepsilon_{ij}\left(\frac{4\sigma_{ij}^{12}}{9r_{\mathrm{c}}^{9}} - \frac{2\sigma_{ij}^{6}}{3r_{\mathrm{c}}^{3}}\right) \quad (29)$$

With these expressions we can obtain the grand-potential of a phase confined in a slit and the pressure of a bulk phase. Where metastable phases exist the equilibrium phase is that with the lowest grand-potential (the highest pressure or average transverse pressure if it is a bulk phase or planar phase respectively).

The angle brackets imply an average obtained from an ensemble of microscopic states. During a Monte Carlo simulation microscopic quantities of interest are calculated and stored at regular intervals. Since it is impossible to generate all members of the ensemble, ensemble averages will always be subject to statistical uncertainties even if there are no systematic errors. The required length of a simulation will depend upon the magnitude of fluctuations in a quantity of interest and the associated level of statistical error that is deemed satisfactory. The statistical error, υ, in a series, η, of uncorrelated values, A_k, is [4,5]

$$\upsilon = \sqrt{\frac{1}{\eta}\sum_{k=1}^{\eta}(A_k - \langle A\rangle)^2} \quad (30)$$

This expression must be divided by $\delta^{1/2}$ if, on average, blocks of length δ of the series are correlated [4,5]. This means that when fluctuations in a quantity are slow the length of the simulation must be increased to achieve a satisfactory level of statistical error.

Systematic errors are often caused by inefficient sampling of microstates, or poor ergodicity. These errors occur when the sampled microstates are not statistically representative of a single thermodynamic state. For example, near the critical temperature of a bulk fluid, the liquid and gas phases in a Gibbs ensemble simulation can "swap" boxes and so neither box can represent one phase only. Alternatively, a poor choice of simulation move might result in rejection of the

overwhelming majority of moves. This can occur in both Gibbs and Grand-canonical ensemble simulations of dense phases where it becomes increasingly unlikely that inter-box, creation and annihilation moves will be accepted as the density of a phase increases. This type of ergodicity deficiency has been called quasi-ergodicity [46].

For the case when more than one thermodynamic state is sampled, a histogram of the relevant order-parameter (for example, the density) will reveal more than one statistically significant peak. When simulating bulk fluid phases, as in the Gibbs ensemble, it can be shown that the locations of these peaks correspond to the equilibrium gas and liquid densities. Thus a histogram analysis provides a valuable complement to Eq. (31) (for a much more detailed discussion, see Ref. [6], chapter 6). Various approaches have been developed to combat quasi-ergodicity including cavity biased [47] and configurational biased sampling [48].

PHASE COEXISTENCE RESULTS

Our goal is to fine-tune effective molecular models of N_2, CO, CH_4 and CO_2 to achieve good agreement between coexisting liquid and gas densities and pressures obtained from Gibbs ensemble simulation and experimental data [33–40]. We perform Gibbs ensemble simulations with N, V and T held constant and for which we first need to choose appropriate values. Clearly, we must set T to be between the appropriate experimental bulk critical point temperature and triple-point temperature. The choice of N and V is less straightforward. V should be chosen so that the instantaneous box length side, L, is always greater than twice the cut-off length, r_c. N is chosen so that the volumes of the two simulation boxes are approximately equal at equilibrium. L determines the maximum spatial correlation length obtainable by a system and this in turn affects the location of

TABLE I Model parameters for gas–gas interactions

Parameter	*N_2*	*CH_4*	*CO*	*CO_2*
σ_{ff} (nm)	0.334	0.373	C:0.349 O:0.313	C:0.275 O:0.3015
ε_{ff}/k_B(K)	34.7	147.5	C:22.8 O:63.5	C:28.3 O: 81.0
l_x (nm)	±0.05047	0	C:+0.056 O:−0.056	C:0 O:±0.1149
l_q (nm)	±0.0847 ±0.1044	0	C:+0.056 O:−0.056	C:0 O:±0.1149
$q(e)$	0.373 −0.373	0	C:0.0203 O:−0.0203	C:0.6512 O:−0.3256

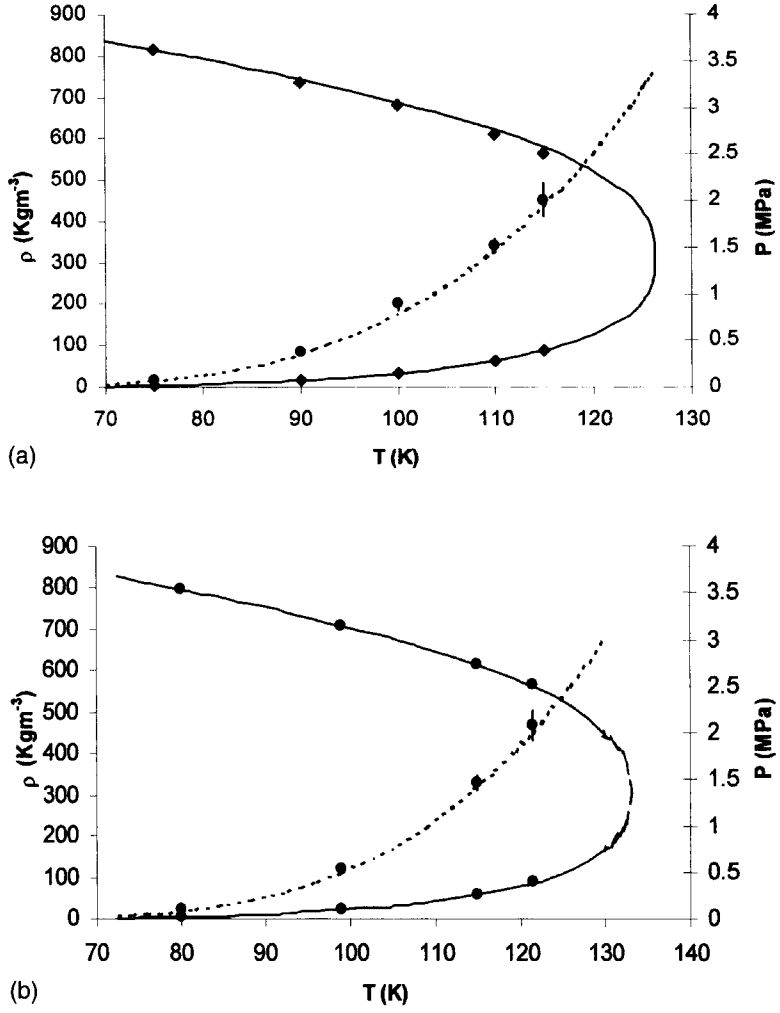

FIGURE 2 (caption opposite)

the bulk critical point. So N, V and the critical-point are affected by our choice of cut-off.

We set $r_c = 1.5\,\text{nm}$ and employ long-range LJ corrections [49] in all simulations. We calculate the pressure of each phase according to Eqs. (29) and (30) and calculate statistical errors from Eq. (30). The best-fit molecular models are described in Table I. The liquid and gas coexisting densities and pressures are presented in Fig. 2a–d. We note that, rather than performing additional Gibbs ensemble simulations for CH_4 in this work, we have instead fine-tuned the model

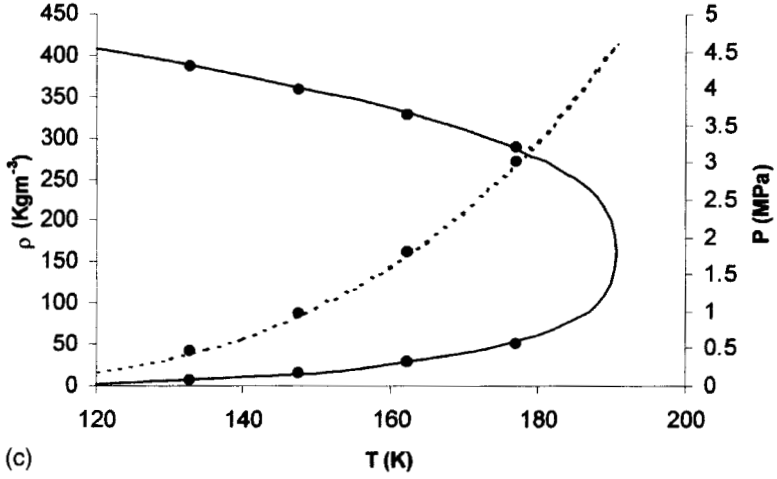

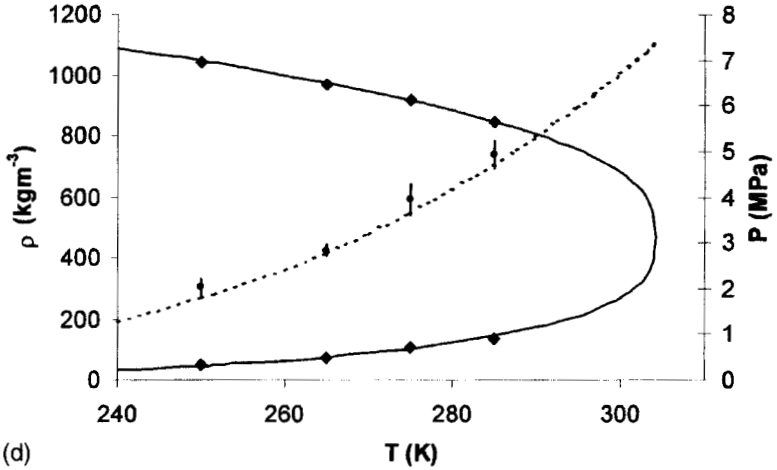

FIGURE 2 Coexistence properties of; a) N_2, b) CO, c) CH_4 and d) CO_2. Lines are experimental data (see text) and symbols are results from Gibbs ensemble simulations except for c) where symbols are results from the EOS of Kolafa and Nezbeda [50] for a LJ fluid. All model parameters are given in Table I. The experimental density data has been extrapolated to the critical point in b) (long-dashed line).

parameters by fitting an equation-of-state [50] (EOS) for the Lennard–Jones fluid to the reference coexistence data at several temperatures below the critical temperature. We use the EOS of Nezbeda and Kolafa [50], which is obtained by fitting to simulation results from a wide range of sources and is thought to accurately predict coexistence pressures and densities.

Because of the relatively large cut-off used our simulations generally hold relatively large numbers of molecules. These molecular models might not be the most efficient computationally since it is possible that effective molecular models can be found which employ a smaller cut-off and fit the reference data equally well.

ISOTHERM RESULTS

The next step is to fine-tune effective molecular models of N_2, CO, CH_4 and CO_2 adsorbed on graphitic surfaces to achieve good agreement between adsorption isotherms obtained from Grand-canonical ensemble simulation and experimental data on reference materials. We perform Grand-canonical ensemble simulations with μ, A, w and T held constant. Our choice for μ, w and T is determined by available experimental data. We need to choose an appropriate value for $A = L^2$. Clearly, L should always be greater than twice the cut-off length, r_c. Also, L determines the maximum transverse spatial correlation length obtainable by a system and this in turn affects the nature of critical phenomena in adsorbed fluids, such as in wetting films.

In previous work [30,31] we calibrated appropriate values for ε_{ss}, for the interaction of N_2 at 77 K and N_2, CH_4 and CO_2 at 298 K with a graphitic surface. We use the same values for CO_2 on graphite at 273 K as for 298 K. We take σ_{ss} to be 0.34 nm, a commonly used value [27,51]. The individual site-surface interaction parameters, ε_{is}, and σ_{is}, are recovered with the Lorentz–Berthelot rules (3). The appropriate values for ε_{ss} and σ_{ss}, for the interaction of CO at 298 K with a graphitic surface are assumed to be identical to those for N_2 at 298 K. To be consistent with our Gibbs ensemble calculations we use the same molecular models (described in Table I) and employ long-range corrections for LJ interactions only. The gas-surface interaction parameter values are presented in Table II.

TABLE II Model parameters for gas–solid surface interactions

Parameter	*N_2*	*CH_4*	*CO*	*CO_2*
σ_{sf} (nm)	0.337	0.365	C:0.3445 O:0.3265	C:0.308 O:0.321
ε_{sf}/k_B (K)	26.0	54.3	C:21.1 O:35.2	C:23.8 O:39.2
ε_{ss}/k_B (K)	19.5	20	C:19.5 O:19.5	C:19 O:19

Figure 3a–d shows adsorption isotherm databases for N_2 at 77 K up to 1 bar, CO and CH_4 at 298 K and CO_2 at 273 K in graphitic slit pores. We calculate bulk pressures using Eqs. (29) and (30). At these temperatures N_2 is significantly sub-critical, CO and CH_4 are significantly super-critical and CO_2 is marginally sub-critical. Because of this temperature range the databases in Fig. 3a–d show a wide range of phenomena. All the databases show adsorption generally increasing with pressure. The CO and CH_4 databases exhibit high adsorption for narrow pore widths indicative of the strongly attractive nature of the graphitic pore walls. The CH_4 database also shows a secondary maximum for adsorption at high pressure in pores able to accommodate two layers of adsorbate. This secondary maximum appears as a slight bump in the CO database, which is more supercritical than CH_4 at 298 K. But both these databases are quite featureless for higher pore widths.

The CO_2 database contains much more information than the CO and CH_4 databases. Adsorption in pores that can accept one layer of fluid only is almost "flat" at high pressure indicating that these pores are nearly saturated. The secondary maximum indicating two adsorbed layers extends to wider pores and capillary condensation is observed for the widest pores at pressures close to saturation.

Nitrogen at 77 K is closer to its triple point temperature (63 K) than its critical temperature (126 K). This is reflected in the complexity of the N_2 (77 K) database. This sensitivity of the pore density to pore width makes N_2 at 77 K an attractive choice for pore size characterisation studies for a wide range of materials. We see that the narrowest pores are saturated with N_2 even for very low under-saturated pressures. For wider slits we see capillary condensation for a wide range of slit widths. For wide slits a N_2 monolayer forms at about $P = 0.001$ bar prior to condensation at higher pressure. However, capillary condensation appears to vanish for $1.2\,\text{nm} < w < 1.7\,\text{nm}$ and then re-appear for $1.0\,\text{nm} < w < 1.2\,\text{nm}$ before vanishing again in smaller pores. This apparent "re-entrant" capillary condensation is probably caused by packing effects that disrupt condensation for $1.2\,\text{nm} < w < 1.7\,\text{nm}$ and enhance it for $1.0\,\text{nm} < w < 1.2\,\text{nm}$. This phenomenon has been observed before [17] in DFT and simulations studies of spherical N_2 molecules. Packing effects are also responsible for the oscillations in average pore density with slit width in the condensed region of the database.

Each database result is obtained with a Grand-canonical ensemble simulation initialised with zero molecules. Due to the high free-energy barrier between gas-like (monolayer) and liquid-like (capillary condensed) states such simulations are unlikely to sample microstates corresponding to liquid-like states if the bulk pressure is too close to the capillary condensation transition pressure, P_{cc}. This means that we need to perform additional simulations initialised with liquid-like configurations to determine the properties of the liquid-like branch of the isotherm in this region. Coexisting gas-like and liquid-like states can then be

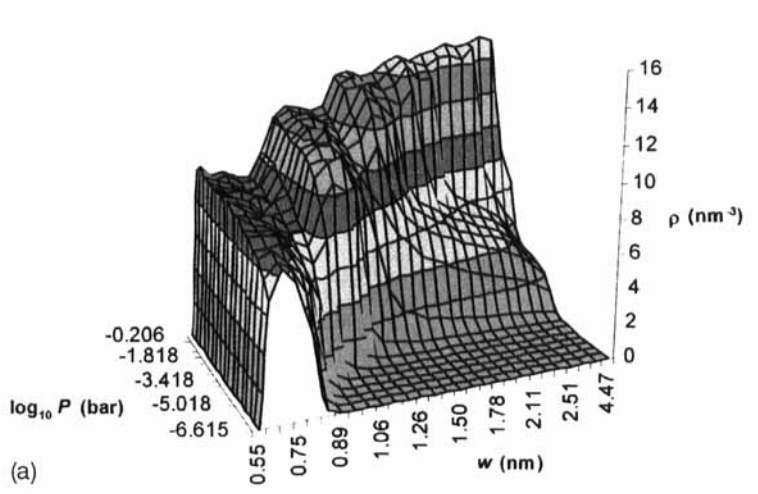

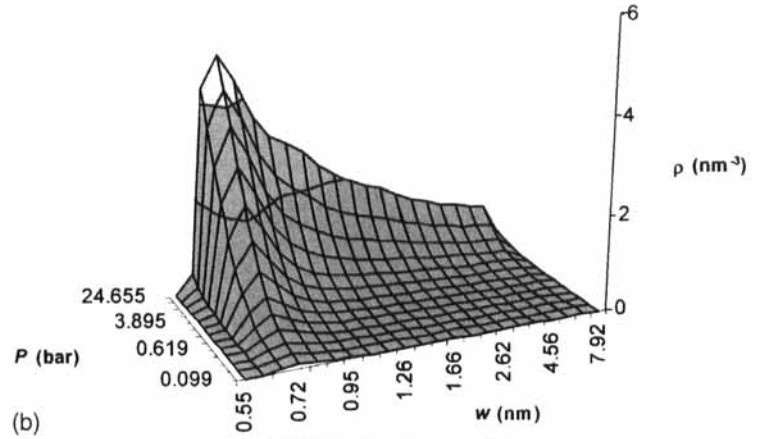

FIGURE 3 (caption opposite)

determined by calculating when the grand potential (or the average transverse pressure) on each isotherm branch is equal [52]. To provide an example of this procedure we have located P_{cc} for $w = 2.512\,\text{nm}$. We calculate the grand-potential by integrating the Gibbs adsorption Eq. (22) along each branch. The constant of integration for each branch is determined at a single point using the virial expressions (27) and (28). Figure 4 shows the results of these calculations and also verifies that the Gibbs adsorption and virial routes to the grand potential are consistent. We find that $P_{cc} = 0.2 \pm 0.05$ bar for N_2 at 77 K in a graphitic slit of width $w = 2.512\,\text{nm}$. Figure 5 shows the gas-like and liquid-like singlet

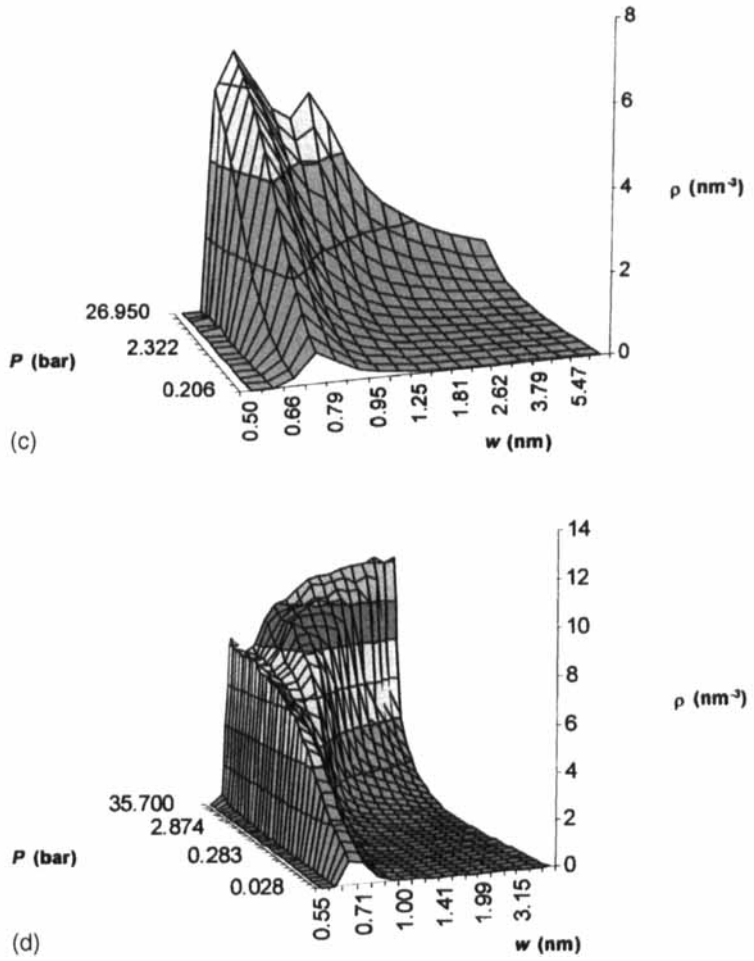

FIGURE 3 Adsorption database for; a) N_2 at 77 K, b) CO at 298 K, c) CH_4 at 298 K and d) CO_2 at 273 K, in graphitic slit pores from Grand-canonical ensemble simulation. Note that P and w are shown on logarithmic scales, except for a) where $\log_{10}P$ (bar) is shown on a uniform scale.

densities (density profiles) for N_2 molecule centres at $P = 0.019$ bar. It is clear that upon condensation the density in the central region of the slit attains liquid-like values. We can also see that the N_2 layers closest to the slit walls are effectively separate from the rest of the fluid.

The N_2 database is not as accurate in the saturated region of isotherms with $w < 1.2$ nm as it is for $w \geq 1.2$ nm because our simulations exhibit quasi-ergodicity in the narrower pores. To illustrate this point we have repeated calculation of the database for $P = 0.01$ bar and a range of values for $w \leq 1.2$ nm

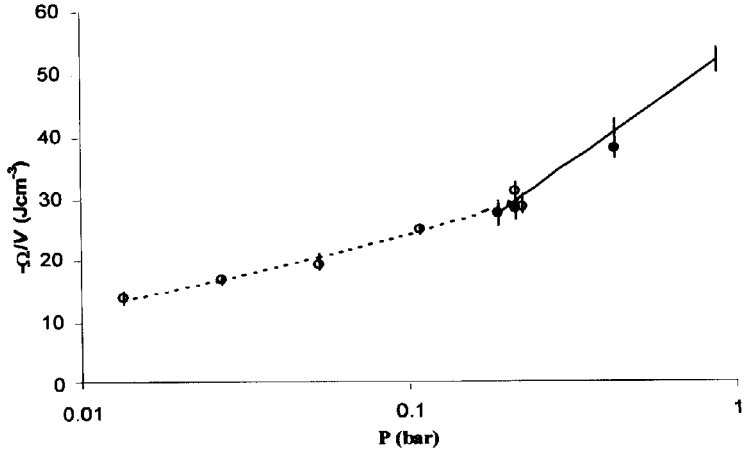

FIGURE 4 Grand potential density isotherms for N_2 at 77 K in a graphitic slit of width 2.512 nm. Lines are calculated from the Gibbs adsorption Eq. (22), symbols from the virial expressions (27) and (28). The dashed line and open symbols indicate gas-like (monolayer) states while the solid line and filled symbols indicate liquid-like (condensed) states. Pressure is on a logarithmic scale.

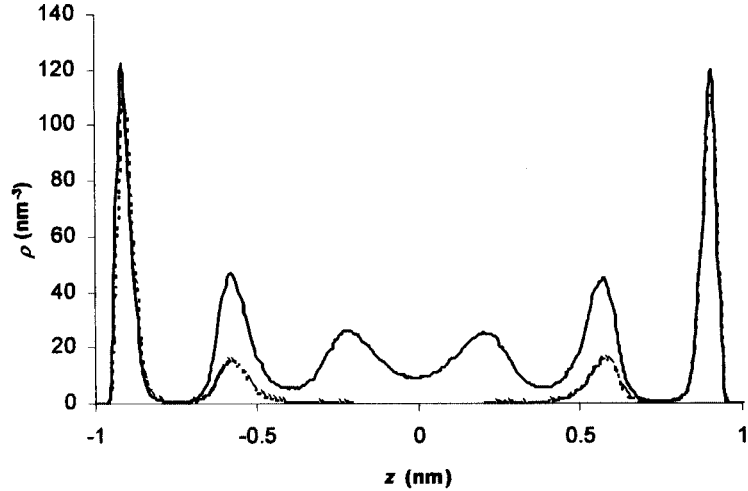

FIGURE 5 Singlet density of N_2 molecule centres at 77 K in a graphitic slit of width 2.512 nm at $P = 0.19$ bar. The solid line is a liquid-like state, the dotted line is a gas-like state and z is relative to the slit centre.

using alternative initial configurations. These initial configurations are generated from the final configuration of simulations in which the N_2—surface interaction strength is gradually reduced from a very high value, to the calibrated value in Table II. So these initial configurations are "over-dense". After simulation of a further 2 million attempted moves, we find that the average pore density is higher

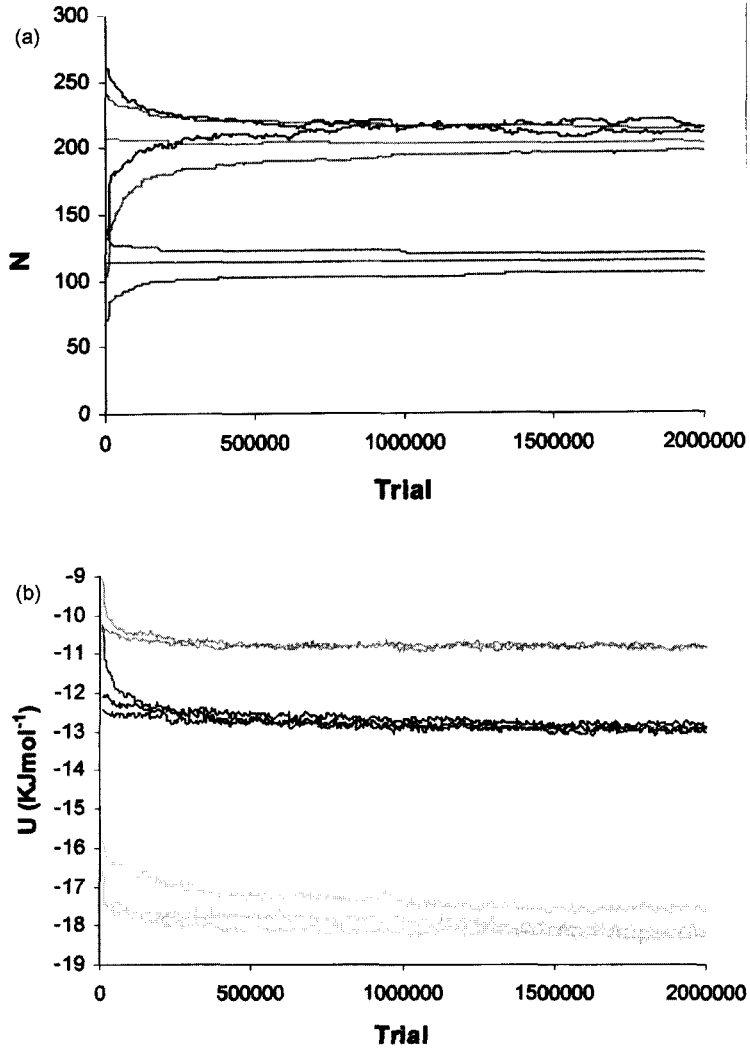

FIGURE 6 (a) Evolution of the number of molecules in Grand-canonical ensemble simulations of N_2 at $P = 0.01$ bar in graphitic slit pores with $w = 0.7$ nm (red lines), 1.0 nm (blue lines) and 1.2 nm (green lines). Lines with the same colour indicate simulations initialised with different states. (b) As for Fig. 6a except that the evolution of the average energy per molecule is shown.

when using an "over-dense" initial configuration compared to an "empty" initial configuration for $w < 1.2$ nm. This indicates quasi-ergodicity for $w < 1.2$ nm resulting from the low probability of acceptance for creation and annihilation moves. We have also performed further simulations with "average-density" initial configurations. The results of these simulations for $w = 0.7$, 1.0 and 1.2 nm

are presented in Fig. 6a,b. They show that equilibrium is attained for $w = 1.2\,\text{nm}$ but not for $w < 1.2\,\text{nm}$. We estimate from these figures that the average pore density in the saturated region of the database for $w < 1.2$ is in error by about 5–10%. It is possible that methods such as the cavity biased method [47] will improve equilibration for $w < 1.2\,\text{nm}$. However, the location of the condensation transition for $w < 1.2\,\text{nm}$ is outside of the quasi-ergodically limited region. This means that we can determine the grand-potential and the location of the phase transition for $w < 1.2\,\text{nm}$. We have performed further simulations at $P = 0.019\,\text{mbar}$ for N_2 in a graphitic slit pores with $w = 1.0\,\text{nm}$. It is clear from these simulations that capillary condensation for $w < 1.2\,\text{nm}$ occurs from a gas-like state to a liquid-like state, albeit with much reduced dimensionality. We are not observing capillary freezing in these slit-pores, although it is conceivable that N_2 does freeze in these pores at higher pressure. Figure 7a,b shows "snapshots" of gas-like and liquid-like metastable states from these simulations.

CHARACTERISATION

The characterisation of porous materials usually involves an approximate solution of the adsorption integral

$$V(P) = A \int f(w) v(w, P)\, \mathrm{d}w \tag{31}$$

where $V(P)$ is the experimentally determined excess volume of adsorbate (at STP) per gram of material, $f(w)$ is the required pore size distribution and $v(w,P)$ is the excess average density of adsorbate at pressure P in a pore of size w. The integral is over all pore sizes, w. Equation (31) is a Fredholm equation of the first kind, and as such it can present many difficulties. Nevertheless several methods for solving Eq. (31) are known including best-fit methods [53,54] and matrix methods [55,56]. The best-fit methods are essentially trial-and-error methods where very many trial functions are tested, with the best-fit trial function taken as the solution. They can employ optimisation procedures to direct the trial function selection towards better solutions. The matrix methods amount to solving a system of linear equations by matrix inversion. With both methods, additional constraints are often required to force more physically appealing or acceptable solutions, including constraints on the smoothness of the solution function and the range of w. Any solution method for Eq. (31) requires that the kernel, $v(w,P)$, is known. The first step is to identify a pore geometry and associated measure, w. With the standard idealised carbon slit-pore model $f(w)$ describes a poly-disperse array of slit pores. Given a fixed geometry, the function v must be calculated for

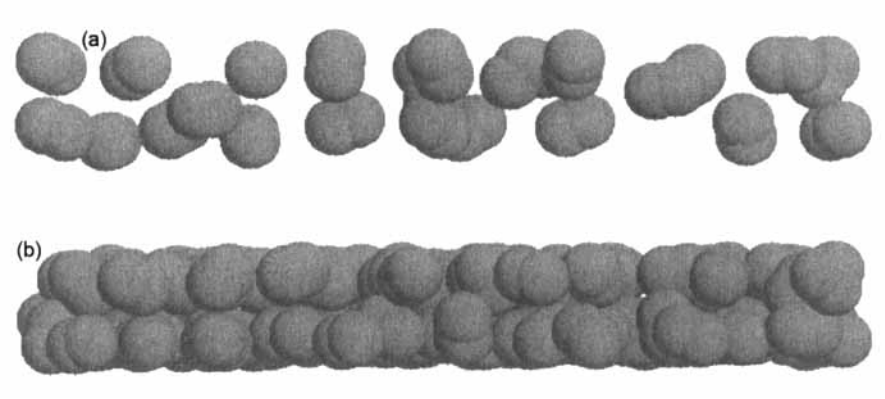

FIGURE 7 (a) A gas-like configuration of N_2 at $P = 0.019$ mbar (close to the capillary condensation pressure) in a graphitic slit with $w = 1.0$ nm. (b) As for Fig. 7a except that a liquid-like configuration is shown.

all relevant values of w and P. The data presented in Fig. 3 constitute $v(w,P)$ for each gas at particular temperatures.

From Fig. 3 it is clear that at 293 K carbon-dioxide adsorption isotherms simulated up to pressures of 30 bar in slit pores are sensitive to slit width. It follows that for our model polydisperse slit pore material the predicted total isotherm will be sensitive to small variations in the PSD. As a consequence the PSD obtained by inverting Eq. (31) will be well constrained by the experimental isotherm. Therefore at room temperature carbon-dioxide will be a sensitive probe of the PSD of porous materials if measurements are made up to the saturation pressure. Carbon-monoxide and methane are supercritical at 298 K; the isotherms are only weak functions of pore width, and hence they are not as sensitive as carbon-dioxide as probes of the microstructure. Clearly, nitrogen isotherms at 77 K (Fig. 3a) are the most sensitive to changes in pore width. However a significant body of theoretical and experimental evidence [57] points to the fact that experimental studies are hampered by very slow diffusion of N_2 into these materials. As discussed above, the database for nitrogen in the important range $w < 1.2$ nm is likely to be inaccurate due to quasi-ergodicity. In this case, with systematic errors in both experimental and modelling data, the pore size distribution obtained from a nitrogen isotherm at 77 K using Eq. (31) is likely to be unreliable for microporous carbon materials.

SUMMARY

We have given an overview of current modelling procedures used to predict the adsorption of a range of gases in graphitic pores complementary to that of

Nicholson [58]. The adsorbed fluids display a wide variety of adsorption behaviours in small pores depending on their interaction potentials and the temperature. From our data we see that at or near room temperature the CO_2 database of isotherms contains much more information than the CO and CH_4 databases. Therefore at room temperature carbon-dioxide will be a sensitive probe of the pore size distribution of porous materials if measurements are made up to the saturation pressure. Nitrogen at 77 K is closer to its triple point temperature (63 K) than its critical temperature (126 K). This is reflected in the complexity of the N_2 (77 K) database. This sensitivity of the pore density to pore width in principle makes nitrogen at 77 K an attractive choice for pore size characterisation studies for a wide range of materials. However both the experimental isotherms and the simulation database are likely to be inaccurate due to the possibility that the equilibrium state of nitrogen in the smallest pores or near pore junctions is solid. Clearly the safest choice is to characterise nanoporous materials using carbon dioxide isotherms at room temperature. Given accurate potentials the techniques discussed here can be used to predict adsorption selectivity both for single pores [59–61] and for an assembly of pores representing the pore size distribution of a real material [62]. An interesting extension of the present work will be to consider the phase behaviour, structure and transport properties of gas mixtures containing water in graphitic nanopores building on the work of Nicholson and colleagues [63].

Acknowledgements

It is a great pleasure for us to acknowledge many years of useful discussions with David Nicholson. As is clear from the many references to his work in the present article he has been a pioneer in the application of molecular simulation methods to the study of physical adsorption. We thank EPSRC for support through grant GR/M94427.

References

[1] Gregg, S.J. and Sing, K.S.W. (1991) Adsorption, Surface Area and Porosity, 2nd ed. (Academic Press, New York).
[2] Rouquerol, F., Rouquerol, J. and Sing, K. (1999) Adsorption by Powders and Porous Solids (Academic Press, New York).
[3] See Evans, R. in (1992) Fundamentals of Inhomogeneous Fluids, Henderson, D. ed, (Dekker, New York), for a detailed survey.
[4] Allen, M.P. and Tildesley, D.J. (1987) Computer Simulation of Liquids (Clarendon Press, Oxford).
[5] Frenkel, D. and Smit, B. (1996) Understanding Molecular Simulation: From Algorithms to Applications (Academic Press, New York).

[6] (1993) Computer Simulation in Chemical Physics NATO ASI Series C: Mathematical and Physical Sciences, Allen, M.P. and Tildesley, D.J., eds, (Kluwer Academic Publishers, Dordrecht) **Vol. 397**.
[7] Rowley, L.A., Nicholson, D. and Parsonage, N.G. (1976) "Grand ensemble Monte Carlo studies of physical adsorption I. Results for multilayer adsorption of 12-6 argon in the field of a plane homogeneous solid", *Mol. Phys.* **31**, 365.
[8] Metropolis, N., Rosenbluth, A.W., Rosenbluth, M.N., Teller, A.H. and Teller, E., "Equation of state calculations by fast computing machines", *J. Chem. Phys.* **21**, 1087.
[9] Norman, G.E. and Filinov, V.S. (1969) "Investigations of phase transitions by a Monte Carlo method", *High Temp. (USSR)* **7**, 216.
[10] Rowley, L.A., Nicholson, D. and Parsonage, N.G. (1975) "Monte Carlo grand canonical ensemble calculation in a gas–liquid transition region for 12-6 argon", *J. Comput. Phys.* **17**, 401.
[11] Adams, D.J. (1975) "Grand-canonical ensemble Monte Carlo for a Lennard–Jones fluid", *Mol. Phys.* **29**, 307.
[12] Israelachvili, J. and Gourdon, D. (2001) "Liquids—putting liquids under molecular-scale confinement", *Science* **292**, 867.
[13] Panagiotopoulos, A.Z. (1987) "Direct determination of phase coexistence properties of fluids by Monte Carlo simulation in a new ensemble", *Mol. Phys.* **61**, 813.
[14] Panagiotopoulos, A.Z., Quirke, N., Stapleton, M. and Tildesley, D.J. (1988) "Phase equilibria by simulation in the Gibbs ensemble: alternative derivation, generalization and application to mixture and membrane equilibria", *Mol. Phys.* **63**, 527.
[15] Smit, B., de Smedt, P.H. and Frenkel, D. (1989) "Computer simulations in the Gibbs ensemble", *Mol. Phys.* **68**, 931.
[16] Panagiotopoulos, A.Z. (1987) "Adsorption and capillary condensation of fluids in cylindrical pores by Monte Carlo simulation in the Gibbs ensemble", *Mol. Phys.* **62**, 701.
[17] Lastoskie, C., Gubbins, K.E. and Quirke, N. (1993) "Pore size heterogeneity and the carbon slit pore: a density functional theory model", *Langmuir* **9**, 2693.
[18] Cracknell, R.F., Nicholson, D., Tennison, S.R. and Bromhead, J. (1996) "Adsorption and selectivity of carbon-dioxide with methane and nitrogen in slit-shaped carbonaceous micropores: simulation and experiment", *Adsorption* **2**, 193.
[19] Nicholson, D. and Gubbins, K.E. (1996) "Separation of carbon-dioxide-methane mixtures by adsorption: effects of geometry and energetics on selectivity", *J. Chem. Phys.* **104**, 8126.
[20] Kaneko, K., Cracknell, R.F. and Nicholson, D. (1994) "Nitrogen adsorption in slit pores at ambient-temperatures—comparison of simulation and experiment", *Langmuir* **10**, 4606.
[21] Whitehouse, J.S., Nicholson, D. and Parsonage, N.G. (1983) "A grand ensemble Monte Carlo study of krypton adsorbed on graphite", *Mol. Phys.* **49**, 829.
[22] Nicholson, D. and Parsonage, N.G. (1986) "Simulation studies of the fluid-monolayer transition in argon adsorbed on graphite", *J. Chem. Soc., Faraday Trans.* **2**, 1657.
[23] Ewald, P. (1921) "Die Berechnung optischer und elektrostatischer Gitterpotemtiale", *Ann. Phys.* **64**, 253.
[24] Heyes, D.M. (1981) "Electrostatic potentials and fields in infinite point charge lattices", *J. Chem. Phys.* **74**, 1924.
[25] Heyes, D.M. (1983) "MD incorporating Ewald summations on partial charge polyatomic systems", *CCP5 Quarterly* **8**, 29.
[26] Barker, J.A. and Watts, R.O. (1973) "Monte Carlo studies of the dielectric properties of water-like molecules", *Mol. Phys.* **26**, 789.
[27] Steele, W.A. (1973) "The physical interaction of gases with crystalline solids", *Surf. Sci.* **36**, 317.
[28] Hanson, J.P. and McDonald, I.R. (1986) Theory of Simple Liquids, 2nd ed. (Academic Press, New York).
[29] Leckner, J. (1991) "Summation of coulomb fields in computer-simulated disordered systems", *Physica A* **176**, 485.
[30] Sweatman, M.B. and Quirke, N. (2001) "Characterization of porous materials by gas adsorption at ambient temperatures and high pressure", *J. Phys. Chem. B* **105**, 1403.
[31] Sweatman, M.B. and Quirke, N. (2001) "The characterization of porous materials by gas adsorption: comparison of nitrogen at 77 K and carbon-dioxide at 298 K for activated carbon", *Langmuir*, (in press).

[32] Sokhan, V.P., Nicholson, D. and Quirke, N. (2000) "Phonon spectra in model carbon nanotubes", *J. Chem. Phys.* **113**, 2007.
[33] Duschek, W., Kleinrahm, R. and Wagner, W. (1990) "Measurement and correlation of the (pressure, density, temperature) relation of carbon-dioxide. 1. The homogeneous gas and liquid regions in the temperature range from 217 K to 340 K at pressures up to 9 MPa", *J. Chem. Therm.* **22**, 827.
[34] Duschek, W., Kleinrahm, R. and Wagner, W. (1990) "Measurement and correlation of the (pressure, density, temperature) relation of carbon-dioxide. 2. Saturated-liquid and saturated-vapour densities and the vapour pressure along the entire coexistence curve", *J. Chem. Therm.* **22**, 841.
[35] Pierperbeck, N., Kleinrahm, R. and Wagner, W. (1991) "Results of (pressure, density, temperature) measurements on methane and on nitrogen in the temperature range from 273.15 K to 323.15 K at pressures up to 12 MPa using a new apparatus for accurate gas-density measurements", *J. Chem. Therm.* **23**, 175.
[36] Handel, G., Kleinrahm, R. and Wagner, W. (1992) "Measurements of the (pressure, density, temperature) relation of methane in the homogeneous gas and liquid regions in the temperature range from 100 K to 260 K and at pressures up to 8 MPa", *J. Chem. Therm.* **24**, 685.
[37] Gilgen, R., Kleinrahm, R. and Wagner, W. (1992) "Supplementary measurements of the (pressure, density, temperature) relation of carbon-dioxide in the homogeneous region at temperatures from 220 K to 360 K and pressures up to 13 MPa", *J. Chem. Therm.* **24**, 1243.
[38] Nowak, P., Kleinrahm, R. and Wagner, W. (1997) "Measurement and correlation of the (P, rho, T) relation of nitrogen. 2. Saturated-liquid and saturated-vapour densities and vapour pressures along the entire coexistence curve", *J. Chem. Therm.* **29**, 1157.
[39] Wagner, W. and de Reuck, K.M. (1996) International Thermodynamic Tables of the Fluid State. 13, Methane IUPAC Chemical Data Series No. 41, (IUPAC, Oxford).
[40] Din, F. (1956) Thermodynamic Functions of Gases Ammonia, carbon-dioxide and carbon-monoxide, (Butterworths, London) **Vol. 1**.
[41] Callen, H.B. (1985) Thermodynamics and an Introduction to Thermostatistics, 2nd ed. (Wiley, New York).
[42] Rowlinson, J.S. and Widom, B. (1989) Molecular Theory of Capillarity (Clarendon Press, Oxford).
[43] Nicholson, D. and Parsonage, N.G. (1982) Computer Simulation and the Statistical Mechanics of Adsorption (Academic Press, New York).
[44] Henderson, J.R. in (1992) "Fundamentals of Inhomogeneous Fluids", Henderson, D., ed, (Dekker, New York).
[45] Alejandre, J., Tildesley, D.J. and Chapela, G.A. (1995) "Molecular dynamics simulation of the orthobaric densities and surface tension of water", *J. Chem. Phys.* **102**, 4574.
[46] Valleau, J.P. and Whittington, S.G. (1986) Statistical Mechanics (Plenum Press, New York).
[47] Mezei, M. (1980) "A cavity biased ($TV\mu$) Monte Carlo method for the computer simulation of fluids", *Mol. Phys.* **40**, 901.
[48] Cracknell, R.F., Nicholson, D., Parsonage, N.G. and Evans, H. (1990) "Rotational insertion bias—a novel method for simulating dense phases of structured particles, with particular application to water", *Mol. Phys.* **71**, 931.
[49] Rowley, L.A., Nicholson, D. and Parsonage, N.G. (1978) "Long-range corrections to Grand-canonical ensemble Monte Carlo calculations for adsorption systems", *J. Comput. Phys.* **26**, 66.
[50] Kolafa, J. and Nezbeda, I. (1994) "The Lennard–Jones fluid—an accurate analytic and theoretically based equation of state", *Fluid Phase Equilibr.* **100**, 1.
[51] Hirschfelder, J.O., Curtiss, C.F. and Bird, R.B. (1964) Molecular Theory of Gases and Liquids (Wiley, New York).
[52] Walton, J.P.R.B. and Quirke, N. (1989) "Capillary condensation: a molecular simulation study", *Mol. Sim.* **2**, 361.
[53] Seaton, N.A., Walton, J.P.R.B. and Quirke, N. (1989) "A new analysis method for the determination of the pore size distribution of porous carbons from nitrogen adsorption measurements", *Carbon* **27**, 853.
[54] Scaife, S., Kluson, P. and Quirke, N. (1999) "Characterisation of porous materials by gas adsorption", *J. Phys. Chem. B* **104**, 313.
[55] Ravikovitch, P.I., Vishnyakov, A., Russo, R. and Neimark, A.V. (2000), *Langmuir* **16**, 2311.

[56] Gusev, V.Y., O'Brien, J.A. and Seaton, N.A. (1997), *Langmuir* **13**, 2815.
[57] Garcia-Martinez, J., Cazorla-Amoros, D. and Linares-Solano, A. (2000), *Stud. Surf. Sci. Catal.* **128**, 485.
[58] Nicholson, D. (1996) "Using computer simulation to study the properties of molecules in micropores", *J. Chem. Soc., Faraday Trans.* **92**, 1.
[59] Cracknell, R.F. and Nicholson, D. (1995) "Adsorption of gas mixtures on solid surfaces, theory and computer simulation", *Adsorption* **1**, 16.
[60] Cracknell, R.F., Nicholson, D. and Quirke, N. (1994) "A Grand-canonical Monte Carlo study of Lennard–Jones mixtures in slit pores 2. Mixtures of 2 centre ethane with methane", *Mol. Sim.* **13**, 161.
[61] Cracknell, R.F., Nicholson, D. and Quirke, N. (1993) "A Grand-canonical Monte Carlo study of Lennard–Jones mixtures in slit pores", *Mol. Phys.* **80**, 885.
[62] Kluson, P., Scaife, S. and Quirke, N. (2000) "The Design of Microporous Graphitic Adsorbents for Selective Separation of Gases", *Separat. Purificat. Rev.* **20**, 15.
[63] Christou, N.I., Whitehouse, J.S., Nicholson, D. and Parsonage, N.G. (1981) "A Monte Carlo study of fluid water in contact with structureless walls", *R. Soc. Chem. Faraday Symp.* **16**, 139.